In situ determinations of the wear surfaces, volumes and kinetics of repassivation: Contribution in the understanding of the tribocorrosion behaviour of a ferritic stainless steel in various pH

V. Dalbert, Nicolas Mary, Bernard Normand, Catherine Verdu, S. Saedlou

In situ determinations of the wear surfaces, volumes and kinetics of repassivation: contribution in the understanding of the tribocorrosion behaviour of a ferritic stainless steel in various pH.

V. Dalbert[1], N. Mary[1,2], B. Normand[1], C. Verdu[1], S. Saedlou[3],

1 Université de Lyon, INSA Lyon, CNRS, MATEIS UMR 5510, F-69621 Villeurbanne Cedex France

2 ELyTMaX UMI 3757, CNRS, Université de Lyon, Tohoku University, Sendai, Japan

3 APERAM Research Center, rue Roger Salengro BP15, F-62330 Isbergues, France

Abstract

In tribocorrosion, the mechanic dominates the total wear. However, the corrosion wear should not be neglected for passive materials. As the film reactivity depends on pH, tribocorrosion experiments were performed on a ferritic stainless steel in sulphate solution (pH 1.5, 6.5 or 12.5). The passive film formation and degradation was evaluated through galvanic coupling tests while the degradation is quantified by image analysis. Wear results follows the Archard's law however, a non-linear dependence of the Archard's coefficient to the pH is found. The study of the worn surface reactivity highlights the role of the pH in the wear behaviour of the material as its influence on the film rebuilt kinetics and its contribution in the total wear.

Keywords: Archard's law; repassivation kinetic; in situ analysis; pH dependence

Highlights:

- The wear volume increases linearly with sliding time as proposed by Archard's law irrespectively to pH.
- The Archard's coefficient is not a simple proportionality factor and depends on the chemistry of the environment and it is not a linear function of pH.
- The wear accelerated corrosion has a greater influence in acidic solution than in neutral and basic solution.
- The repassivation rate is influenced by the redox potential of the surface and also the nature of the passive layer formed.

1- Introduction

Tribocorrosion is a complex process in which mechanical and chemical loads act synergistically on material damages. Consequently, tribocorrosion is greater than tribological or chemical damages considered separately. The quantification of the tribocorrosion is usually based on the amount of matter loss after sliding. From empirical assumptions, different models link the wear to physical parameters [1] [2]. Among them, the Archard's law assumes a linear evolution of the wear volume as a function of the sliding distance, the normal load and the flow pressure (equivalent to the hardness) [3]. As the contact properties also depend on the geometries (general shape of the contact and surface roughness), a coefficient was introduced (named Archard's coefficient).

Several tribocorrosion studies emphasis that the wear resistance is not an intrinsic property of the material and the passive layer has to be considered [4]. As examples, Garcia et al. [5] highlighted the existence of a load domain where an increase of the normal load promotes the wear of an austenitic stainless steel immerged in acidic solution. In this domain, the passive layer of few nanometer thick affects the plastic deformation behavior of subsurface and the wear consequently [6]. Dalbert et al. [7] showed that the field of plastic deformation increases with the repassivation kinetics which modifies the mechanical properties of the material and enhances the wear resistance. Jemmely et al. [8] demonstrate that the wear loss in acidic solution is superior than in basic solution for a ferritic stainless steel. The main reason comes from the different chemical compositions of the passive layers which play a role in the degradation mechanism [4]. On stainless steel, the nature of the passive film mainly depends on internal (material chemistry) and external factors. The latter is defined by the oxidant power of the solution where pH plays a significant role among other parameters (dissolve dioxygen concentration, anionic species, etc.) [9–11]. In acidic solution, a chromium oxide layer grows on the metal substrate while hydroxide species are detected in very low quantities [12]. When the pH increases, iron contributes to the passive layer and hydroxide concentration increases [13,14]. The solubility of hydroxide species is also affected by changes in pH, and larger quantities are usually found in basic solution rather than in acidic environment [10]. Since the passive film is at the interface between the first body and the counter body surface in tribocorrosion, any modifications in its

hardness (pure chromium oxide or mix chromium-iron oxide), its surface energy (oxide, hydroxide species) may change the physical-chemical properties of the contact and as the result the wear behavior.

Most of these studies performed in potentiostatic conditions attended to describe and to quantify the corrosion-wear behavior of a material. However, Open Circuit Potential tests are still preferred to investigate the wear mechanism under more realistic conditions. The main limitation to the OCP tests is the qualitative description of the surface reactivity from the potential evolution [15]. Thus, modeling approaches coupled with experiments were developed to quantify the wear-accelerated corrosion [9,16]. From the modeling viewpoint, Papageorgiou and coworkers [16] highlighted the influence of the ratio of worn and unworn surfaces on the kinetic of the cathodic reaction (i.e., dissolve dioxygen reduction). More recently Gilbert et al. [17] developed a model to take into account the impedance of the worn and unworn surface to predict the potential evolution during fretting corrosion. Irrespective of the model, the current flowing to the wear track is always estimated without experimental comparisons. From the experimental viewpoint, potential and current variations during sliding tests can be quantified using the electrochemical noise (EN) or galvanic coupling (GC) techniques. In those two approaches, the working electrode (i.e., the sample) is connected to a second working electrode (of a similar or different nature) through a Zero-Resistance Ammeter (ZRA). The potential shown corresponds to working electrode. In absence of sliding, the potential steady state and current are controlled by (i) the potential difference between the two working electrodes, (ii) the oxidant power of the solution and (iii) the surface ratio between the two electrodes. In the EN approach, the signal processing is based on a frequency analysis. The power spectral density (PSD) is extracted from the fluctuations of the potential and the current and gives characteristic curves depending on the corrosion mode [18]. Since high frequency measurements are performed, fast reactions can be described such as the double layer capacitance charging or the depassivation/repassivation rates of the wear track [19]. In the GC tests, current transients are mostly analyzed in the time domain [20–23]. The current envelop is a function of the aggressiveness of the solution, the characteristics of the mechanical contact (normal force, stroke velocity, etc.) and the chemistry of material [20–23]. In both the EN and GC approaches, the design of the tribocorrosion cell is of a great importance to record the current and

the potential in optimum conditions. The distance between the working electrode and the second working electrode should to be controlled with regard to current field lines [24]. The surrounding area of the track should be insulated to force the galvanic coupling between the working electrode and the second working electrode [25]. The cathodic surface defined by the second working electrode should be significantly larger than the anodic surface (i.e., the wear track) [16,26]. The tribocorrosion cell optimization concerns also the chemistry of the second working electrode. Wu et al. [27] demonstrated that a microelectrode in platinum is more suitable than a microelectrode made with material of the working electrode. All these achievements highlight that galvanic coupling techniques are powerful tools to characterize the reactivity of the worn surface during sliding even if they might introduce a bias more a less important in the electrochemical response compare to OCP measurements.

Based on all those considerations, this study aims to discuss the corrosion wear behavior of a ferritic stainless steel immersed into three different solutions pH from galvanic coupling measurements with an emphasis place on:

- The correlation between the volume of matter loss as a function of the solution. For that purpose, an optical microscope will be added to the tribocorrosion in order to precisely quantify at each moment of sliding the wear and to discuss the Archard's law validity. The methodology for the wear surface and volume determination from optical observation is proposed thereafter
- The relation between of the Archard coefficient defined from the previous quantification to the solution pH and look into the mechanical – chemical character of this coefficient.
- The influence of the pH on the repassivation kinetics of the wear track and the contribution of the passive rebuilt in the wear of the material [7].

2. Experimental part and method.

2.1. Specimens, surface preparation and electrochemical characterizations.

This study was performed on a commercial ferritic stainless steel (AISI430) with a chemical composition of 0.03 wt% C, 16.10 wt% Cr, 0.20 wt% Ni, 0.49 wt% Si, balanced with Fe. All samples

were mechanically grounded with Silicon Carbide emery papers (from 800 to 4000 grit), polished with diamond paste from 3 µm to 1 µm ($R_a \approx 0.1 \pm 0.05$ µm) and then cleaned in pure water, and ultrasonically rinsed in alcohol solution during 2 min. After that, the samples were stored for 24 h in a dryer to stabilize the native passive film.

Electrochemical measurements and tribocorrosion tests were performed in an aerated 0.1 M Na_2SO_4 solution (volume of electrolyte equal to 40 mL) with pH values of 1.5 (addition of H_2SO_4), 6.5 (natural solution pH), and 12.5 (addition of NaOH). The solution conductivities were equals to 4.2 S/m, 2.6 S/m and 3.3 S/m at pH 1.5, pH 6.5 and pH 12.5, respectively. For each solution, the passivation ability was determined from the polarization curves recorded from -1.1 V/MSE (cathodic domain) to 0.2 V/MSE (anodic domain) at a sweep rate of 1 mV/s. All potentials were referred to a Mercury Sulfate Electrode, MSE (E_{MSE} = +0.65 V versus the Normal Hydrogen Electrode) and a graphite sheet of 8 cm^2 was used as counter electrode. Prior to the corrosion or tribocorrosion measurements, a cathodic polarization for 30 min at an applied potential of −1.05 V/MSE was applied to stabilize the passive film and to increase the electrochemical experiments reproducibility [28].

2.2. Tribocorrosion parameters

Sliding tests were performed with a reciprocating-motion tribometer (TCT2005, Falex Company, Belgium) [29]. The contact was defined by the stainless steel as first body whereas the second body was a corundum pin with a cylindrical diameter of 6 ± 0.2 mm and a 24 ± 2 mm tip curvature radius. The Young's modulus of the AISI430 was about 211 GPa, the Poisson's ratio of 0.3, and hardness about 1.5 ± 0.1 GPa [30]. The Young's modulus of corundum was about 380 ± 20 GPa, a Poisson's ratio of 0.25, and a hardness of 13.0 ± 0.2 GPa. Since the mechanical properties of the corundum pin were higher than the ferritic stainless steel, the wear was expected on the metal specimen. Note that the contact pressure also induced a significant plastic strain that affected the wear behavior of the material [7]. A normal load of 10 N was applied for 2000 motions (i.e., 1000 cycles). When the two bodies were in contact, the Hertz's elastic theory gave a contact pressure of 405 MPa and a theoretical

pin impression of 450 nm in the metal. A stroke length of 10 mm (trapezoidal shape with a sliding speed of 50 mm/s and a sliding time of 0.2 s) was selected to define study passivation and repassivation for an opened contact. The latency period of 5.5 s was settled from the following closing statements (i.e. one sliding is equal to 5.7 seconds). This duration was establish from preliminary experiments and already used in [28]. Note that the ohmic drop was quantified and the potential drift was evaluated at 1×10^{-6} V/MSE and was neglected thereafter [20,21,31,32].

The tribocorrosion experiments were performed in a galvanic coupling cell where the stainless steel (i.e., the working electrode) was connected to a second working electrode in graphite through a Zero Resistance Ammeter (Potentiostat Ref600, Gamry company; USA). The potential of the stainless steel electrode was measured according to a mercury sulphate electrode MSE (reference electrode E=+650 mV/ENH) distant from 1 cm to wear track and located at 5 mm above the metallic surface measured. A schematic representation of the tribocorrosion cell is given in Figure 1 where the graphite electrode with a "half-moon shape" surface (S_{gr} = 8 cm²) faces the AISI430. The working surface area was equal to 10.5 cm^2. The distance between these two electrodes was 5 mm. An optical microscope with a lateral resolution of 0.5 x 0.5 µm² for the camera was implemented to capture images of the wear tracks. In the present study, any potential bias was applied between the reference electrode and the working electrode during the tribocorrosion tests. Therefore, the stainless steel potential resulted to the electrical coupling with the graphite electrode. As graphite is nobler than stainless, anodic reactions were located preferentially on the metallic electrode. Two working electrodes surfaces were not modified between all the tests as well as their positions in the electrochemical cell. Consequently, the stainless steel potential depends of the oxidant power of the solution (i.e., the pH). Potential and current data were recorded with a frequency of 100Hz using the GAMRY ESA410 software. Automatic current range was disable to avoid measurement offset and the current range was fixed to 100 µA. Experiments were performed at least 3 times, and the results shown hereafter represents the average behaviour.

After the tribocorrosion tests, the wear volumes and surfaces ($S_{a,2Dprofil}$) were calculated from contact profilometry measurements (Surfascan 2D, Somicronic, Belgium). Multiple 2D profile lines were

recorded in the perpendicular direction to the sliding and surfaces or volumes were estimated with the method of Qu et Truhan [33]. Additionally, the wear tracks were also examined using a field-emission scanning electron microscope (FE-SEM, Supra 55VP, Zeiss, Germany) to investigate the wear mechanism as a function of pH.

3. Results and discussions

3.1. Microstructure and electrochemical behavior.

Figure1a shows the microstructures of AISI430 after electrochemical etching presented in detail in our previous paper [7]. Typical ferritic microstructure was observed with a grain size in the range of 20–100 µm. The microstructure did not exhibit any particular morphology to the rolling direction. It can be noticed that chromium carbides (black dots) were homogeneously distributed at grain boundaries. A small depletion of the matrix in chromium was estimated to ~1.5 wt%.

The polarization curves in Figure 2b show the dependence of the passivation ability of stainless steel with pH. In acidic solution, the corrosion potential is located at -0.9 V/MSE and an active-passive transition is observed at approximately -0.8 V/MSE. Aboce -0.7 V/MSE the current density reached a passive plateau (~10 µA/cm²). In neutral and basic solutions, the corrosion potentials shift to -0.6 V/MSE and -0.7 V/MSE, respectively. The passive current densities are about 1 µA/cm² and 10 µA/cm² at pH 6.5 and 12.5, respectively. At pH 12.5, the transpassive peak starting at 0.2 VMSE indicated surface activation due to the oxidation of the Cr^{3+} throughout the film in Cr^{6+}. In the cathodic region, the curve at pH 6.5 and pH 12.5 show a quasi-plateau below -0.9 V/MSE related to the mass transport limitation of dissolved oxygen. Therefore, the passivation ability of the sample is not modified by a modification of the pH below -0.1 V/MSE.

3.2. Electrochemical reactivity as a function of the pH.

Figure 3 present the potential (left column) and the current density (right column) variation during the tribocorrosion experiments. When the sliding starts, the potential of the material shifts to higher

cathodic value while the current density increases. After sliding, the potential and current tend to reach their initial values, indicating that the passivation ability of the wear track is not lost. In pH 1.5, the potential under sliding (E_s) is approximately at -0.4 V/MSE whereas E_s are about -0.6 V/MSE and -0.7 V/MSE in the neutral and basic solutions. On one hand, E_s locates in the middle of the passive plateau in acid solution (Figure 2b). On the other hand, E_s is close to the corrosion potential in neutral and basic solutions. As all E_s are in the passive region (see Figure 2b), the electrical charge required to rebuilt the film is linked to the overpotential and may influence the repassivation kinetics of the wear track [34].

In the running-in domain (below ~400 sliding), the maximums of current densities are at approximately 1 $\times 10^{-2}$ A/cm^2, 0.5 $\times 10^{-2}$ A/cm^2, and 0.25 $\times 10^{-2}$ A/cm^2 at the pH 1.5, 6.5, and 12.5, respectively. For the first scratches, the material degradation is directly controlled by the geometry of the asperities of both AISI430 and corundum pin. Micro-cutting is the main mechanism of degradation and leads to a high reactivity of the surface wear track [35]. Above ~400 sliding, the current densities decrease as a function of the reactivity of the surface in the electrolyte. In the linear regime of wear, the maximum contact pressure is located at the edges of the wear track whereas the contact pressure inside the wear track is closed to the yielding stress [36]. As a consequence, the current density is representative to the reactivity of the deformed surface (i.e., inside the contact) and the edges of the wear track freshly damaged.

On Figure 3 (left column), the amplitudes of variation depend on the reactivity of the material in the electrolyte. The current rises during sliding because of the oxide film breakdown and it falls during the latency period because of the film growth (Figure 4a). The film formation is usually resolved into:

- Double layer charging. In the first few µs, the current response is a function of the differential capacitance of the interface and the re-establishment of the ionic species distribution in the double layer [19,37]. Moreover, the sample rate and the trapezoidal motion of the pin are not optimum to detected the double layer charging in our experiments [38].
- 2D mechanism of recovery. Here two processes occur at the same. The film nucleation and 2D grow takes place in parallel to the dissolution of the surface which is not covered by the

protective layer yet [39,40].

- 3D mechanism. This step corresponds to the film thickening until its characteristic length which depends on the ions and the oxide-hydroxide species involved in the growth mechanism.
- Film ageing. Usually, the film ageing or maturation of on stainless steel occurs in few hours [19–23]. The latency period of 5.7s selected in this work is then not suitable to quantify that process. Therefore, the current analysis in this work focuses only on the 2D mechanism and the 3D mechanism of the film recovery [7,21,38,41].

The current fall can be modelled by the sum of two exponentials where τ_{2D} and τ_{3D} are the time constants of the 2D mechanism (film nuclei covering rate) and the 3D mechanism (film thickening), respectively.

$$J_t = J_{2D} + J_{3D} = J'_{2D}.exp\left(-\frac{t}{\tau_{2D}}\right) + J'_{3D}.exp\left(-\frac{t}{\tau_{3D}}\right) + J'_0 \qquad \text{Equation 1.}$$

In Equation 1, J'_{2D} and J'_{3D} are the current amplitudes related to each process and J'_0 represents the limit of the current at the end of the latency period (i.e. the current at the passive steady state). Based on the mixed potential relationship proposed by Fleishmann and Thirsk, Beck expressed the current density fall (J_{2D}) as Equation 2 [42]:

$$J_{2D} = I_{ex}.S.(1-\theta).\exp(\beta_a.\eta) = J'_{2D}.exp\left(-\frac{t}{\tau_{2D}}\right) \qquad \text{Equation 2.}$$

$$\text{With } \theta = 1 - \exp(-k.t^n) = 1 - \exp(-\frac{1}{\tau_{2D}}.t) \qquad \text{Equation.3.}$$

Where, I_{ex} is the exchange current with the bare surface (A), S is the wear track surface (cm²), β_a is the anodic Tafel slope of the bare surface (V^{-1}), η is the overpotential (V) and θ is the surface coverage of oxide nuclei (mono layer). In Avrami' theory, θ is a function of the Avrami exponent n and the constant k which reflects the film formation rate in s^{-n} (Equation 3). n is the reaction order and is equal to 1 for islands growth in 2 dimension [41]. Therefore, k is inversely proportional to τ_{2D} in Equation 3.

Figure 4b presents an example of fit for a transient in acidic solution (stroke n°1800) and also reports the covering rate of the surface by passive nuclei. Note that the surface covering by the film nuclei is a fast process and Equation 1 fits well the current fall and this for the whole transients of this study. Figure 4c and Figure 4d report the variations τ_{2D} and τ_{3D}, respectively. Roughly speaking, τ_{2D} and τ_{3D} are in the range of ~0.2 seconds and ~1.2 seconds, respectively. τ_{2D} values are at least 100 times higher to the time to charge the double layer determined by other authors and are consistent with the characteristic time constants for the nucleation mechanism limited by a charge transfer [26]. Whatever the solution, τ_{2D} and τ_{3D} stabilize after 400 sliding. In the linear regime of wear, τ_{2D} is equal to 0.19 s, 0.3 s and 0.21 s in pH 1.5, pH 6.5 and pH 12.5, respectively. The slowdown of the oxide nuclei germination (τ_{2D}) between pH 1.5 and pH 6.5 comes from the injection of iron oxide in the Cr_2O_3 layer [12]. The lower formation enthalpy of the iron oxide (ΔH_f^θ Fe_2O_3 = - 820 kJ/mol) compared to the chromium oxide (ΔH_f^θ Cr_2O_3 of -1200 kJ/mol) and the smaller overpotential (potential drop during sliding) lead to a lower driving force for the repassivation [43,44]. With the pH increases from 6.5 to 12.5, the hydroxyl part of the oxide film and the solubility limit of either chromium or iron hydroxide have to be considered [45,46]. The precipitation of chromium and iron hydroxides and oxides in basic solution may help the oxide reformation as suggested by the decreases of τ_{2D}. Regarding the film thickening (τ_{3D}), a slowdown in the film thickening occurs above pH 6.5 since hydroxide grow and the film and might change the diffusion of species [47]. The fluctuations in basic solution are associated to the hydroxide oxide nature of the passive layer which could interface properties and might enhance the adhesion forces between the substrate and the pin. The modification of the contact properties by the formation of a strong hydroxide layer is also supported by the higher average coefficient of friction and also the wear track morphology (Figure 6c and Figure 7, respectively).

In order to confirm the mechanical removal of the oxide by the pin sliding, the average film thickness rebuilt for each stroke can be estimated by Equation 4. The oxide thickness varies between 1 and 2.5 nm and is in the same order of magnitude that passive film in aerated solution determined by Olsson et

Stemp [21]. Note that the pin penetration depth is larger than the film thickness which confirms the full depassivation of the surface [21].

$$\xi = \frac{M_{ox\cdot}}{z.F.\rho_{ox}} Q_{3D} = \frac{M_{ox}}{z.F.\rho_{ox}} \int_{t=0.2s}^{t=5s} J_{3D}.dt \qquad \text{Equation. 4}$$

Where M_{ox} is the Cr_2O_3 oxide (152 g/mol), z is the equivalent number of electron involves in the film growth (3), ρ_{ox} is the density of Cr_2O_3 (5.2 g/cm^3) [8,41,48]. Q_{3D} is the electrical charge density involved in the film grow and is equal to the integral of J_{3D} with time.

3.3. Wear surfaces and volumes variation as a function of the pH.

After tribocorrosion tests, the wear surfaces were cleaned with deionized water, pulsed air dried. 2D profiles were recorded to calculate the wear track surface and volume (Figure 5d). Some fluctuations on the profiles are detected in neutral and basic solutions which might come from the presences of a third body in the wear track and its surrounding. Table 1 reports the average values for the surface ($S_{a,2Dprofil}$) and volume ($V_{a,2Dprofil}$) as a function the pH calculated with [33]. As expected, the highest wear occurs in acidic solution (3.8 x 10^{-5} cm^3) while the tests in basic solution mitigate the wear (0.9 x 10^{-5} cm^3) [8].

By the mean of the optical microscope implemented in the tribocellule, images of the wear track were taken continuously during the experiment. Figure 5a and Figure 5b present two snapshots of the wear track in solution pH 1.5 after 180 and 1480 sliding, respectively. On those images, the wear track width, l, can be easily measured and the wear track surface ($S_{a,image}$) estimated for each stroke (Equation 5). The total wear surface $S_{total,image}$ is then the sum of each $S_{a,image}$ (Equation 6). In this study, the wear tracks are approximated by a cylindrical surface with partial spherical surfaces at the extremities (Equation 5) [33,49].

$$S_{a,image} = 2.\pi.R_c.h + 2.R_c.L.\operatorname{asin}\left(\frac{l}{2R_c}\right) \qquad \text{Equation. 5}$$

$$S_{total,image} = \sum_{stroke\ number}(S_{a,image}) \qquad \text{Equation. 6}$$

Where R_c is the pin curvature radius (cm), L is the stroke length (cm), and l is the track width (cm).

In Equation 5, the indent penetration h has to be provided as other parameters are otherwise measured. In the present experiments the corundum pin has the highest hardness, therefore the wear should be mostly sustained by AISI430. Thus, an invariant pin radius (R_c = 24 mm) is considered and the penetration depth h is calculated from Equation 7 [49]. Note that the validity of the assumptions on the pin wear will be discussed later on.

$$h = Rc.\left(1 - \cos\left(asin\left(\frac{l}{2.Rc}\right)\right)\right) \quad \text{Equation. 7}$$

From the optical measurement of the wear track width, the wear volume loss $V_{a,image}$ is quantified of each stroke (Equation 7). As for $S_{a,image}$, the pin deformation is neglected in first approximation in Equation 8. The total wear volume $V_{total,image}$ is then the sum of $V_{a,image}$ along the experiment (Equation 9)

$$V_{a,image} = \pi.h^2.(R_c - h/3) + \frac{h}{6.l}.(3.h^2 + 4.l^2).L \quad \text{Equation.8}$$

$$V_{total,image} = \sum_{stroke\ number}(V_{a,image}) \quad \text{Equation.9}$$

Where h is the pin penetration depth (cm), R_c is the pin curvature radius (cm), L is the stroke length (cm), and l is the track width (cm).

Figure 6a and Figure 6b report the surfaces wear tracks $S_{tot,image}$ and volumes $V_{total,image}$ variations as a function of the pH. Before describing them, the hypothesis on pin wear is verified by a comparison of the wear volumes and surfaces calculated from optical approach with the 2D profilometry measurements. On Table 1, values for the two methods are close in neutral and basic solutions. In pH 1.5, a difference of 3% is calculated however it remains in the error bars of the reproducibility tests. On one hand, the assumption on the pin properties is validated (i.e., mechanically and chemically inert). On the other hand, it allows us to consider the quantifications of surface wear and volume from the optical approach.

In Figure 6a, the variation of the wear surface $S_{total,image}$ with the stroke number can be divided into two regions. Below 300~400 slidings, the wear surface follows a logarithmic evolution for which the wear is mostly controlled by the two bodies surfaces (pin and samples) [50]. Note that the standard deviation leads to some difficulties to clearly detect the role of pH on the damage. In this region, the roughness of the two materials promotes an abrasive contact that enhances the degradation of the material [35,51]. Above 400 slidings, the wear surfaces increase linearly with time in agreement with the linear regime of wear. The slopes ($\Delta S_{total,image}/\Delta t$) express the rate of wear and are equal to 4.4×10^{-6} cm^2/s, 4.0×10^{-6} cm^2/s and 2.7×10^{-6} cm^2/s at pH 1.5, pH 6.5 and pH 12.5, respectively. The decrease of $\Delta S_{total,image}/\Delta t$ with the pH is consistent with the slowdown of the surface reactivity at higher pH [8].

Figure 6b reports the wear volume ($V_{total,image}$) increase with the sliding time and pH. As observed on the wear surface, an increase of pH remains beneficial for the wear reduction. Whatever the test, the volume of loss increases linearly with the sliding as predicted by the Archard's theory [3]. Even if this theory was initially developed for sliding in dry condition, it is often used in tribocorrosion until the mechanical contribution is significantly either than the chemical wear in the degradation mechanism [36,51]. In the Archard's law, the wear volume V_i (m^3) is proportional to the hardness of AISI430, H (Pa or kg.m^{-1}.s^{-2}) and the normal load, F (N or kg.m^{-1}). The proportionality or Archard's coefficient k (m^2.s^{-2}) is expressed as a function of sliding distance d (m) (Equation 12). In this work, the Archard's coefficient is proportional to the slope of the curves in Figure 6b.

$$k_{archard} = \frac{V_i.H}{F.d} \qquad \text{Equation. 10}$$

Figure 6c suggests a nonlinear dependence of $k_{archard}$ with pH. It also highlights that $k_{archard}$ is not a simple proportionality factor with a mechanical origin and includes a chemical contribution related to the nature of the passive layer, the surface reactivity etc. This is also reinforced by the nonlinear evolution of the coefficient of friction as already mentioned (Figure 6c).

After tribocorrosion, the worn surfaces were observed by SEM (Figure 7). The micrographs show several grooves perpendicular to the sliding direction online with an abrasion degradation. The metallurgical state of the wear track depends also on the pH. In acidic solution, a chromium enriched oxide film is expected whereas a mix chromium and iron oxide-hydroxide layer grow in neutral and basic solution. The oxide becomes less brittle with the iron injection and the hydroxide part, a material transfer is observed on the pin surface at pH 6.5 and above (in windows capture, Figure 5) [52–55]. The worn surface partially delaminates in pH 12.5 because of the predominance of the hydroxide nature of the oxide. For this latter, the cross-section SEM image in Figure 7d shows the roughness/waviness of the worn surface partially filled by a third layer enriched in chromium, iron and oxygen (determined by EDS analysis). Even if a hydroxy-oxide layer creates a stronger adhesive interface between the material and the pin at pH 12.5 (Figure 6c), the wear volumes, however, remain lower because of a lower electrochemical reactivity of the surface and a probable higher deformability of the oxide-hydroxide.

3.4. Chemical wear volume

Whatever, the method (optical observation) or 2D profile measure, the total wear at the end of the tribocorrosion test can be easily quantify. Since, the passive film is successively damaged and rebuilt, a non-negligible part of the material dissolve in absence of a protective layer. This is called the chemical wear volume (V_{wac}) and corresponds to the sum of matter release during sliding ($V_{sliding}$) and the repassivation process (2D mechanism, V_{2D}).

$$V_{wac} = V_{sliding} + V_{2D,image} \qquad \text{Equation. 11}$$

In Equation 11, the volume of mater dissolved during the pin motion ($V_{sliding}$) is calculated from the Faraday law (Equation 12). For each current transient, the current rise is associated to the dissolution of the surface under sliding. The electrical charge ($q_{sliding,i}$) or the electrical charge density ($Q_{sliding,i}$) of a single event are calculated from the integration of the current vs time curve (from 0s to 0.2 s, Figure 4a).

$$V_{sliding} = \sum_i q_{sliding,i} \frac{M_{ss}}{z.F.\rho_{ss}}$$ Equation. 12

$$V_{2D,image} = \sum \frac{M_{ss}}{z.F.\rho_{ss}} q_{2D} = \sum \frac{M_{ss}}{z.F.\rho_{ss}} \int_{t=0.2s}^{t=5s} J_{2D}.dt$$ Equation 9

Where M_{ss} is the molar weight of the stainless steel (55 g/mol), z is the charge of the cations (for Fe and Cr, z is equal to 3), ρ_{ss} is the density of the AISI430 (5.5 g/cm^3) and q_{2D} is the electrical charge associated to the dissolution of the surface during the latency period (2D mechanism).

The chemical wear volumes (V_{wac}) calculated by Equation 10 are reported as a function of the stroke number in Figure 8a. As for the total wear volume, V_{wac} increases linearly with the sliding distance. Note that the chemical wear is bigger in pH 1.5 since the dissolution of the material is more significant evenif the surface repassivation is faster. In the total wear volume, the contribution of the chemical wear represents between 10 and 30 % of the volume of material lost (Figure 8b). This percentage remains constant in the linear regime of wear and depends of the solution: lower the pH is, higher V_{wac} will be.

4. Conclusions

In situ wear and electrochemical measurements were simultaneously carried out to discuss the tribocorrosion behaviour of a ferritic stainless steel coupled with a graphite electrode. Experiments were performed in acid, neutral and basic 0.1M Na_2SO_4 solutions. This paper confirms the total wear follows the Archard's law. It also corroborates that the wear rate is controlled by the pH. However, the Archard's coefficient is not a linear function of the pH since the passive film changes in terms of chemistry with pH: iron injection in the chromium layer and stability of hydroxide layer in basic solution. The solution pH is also a key parameter in the kinetics of the oxide growth. The overall repassivation is faster in acidic solution than in neutral solution. This was attributed to the iron stabilisation in the oxide layer. In basic solution, the solubility limit of hydroxide species has to be considered as an agent of repassivation.

5- Bibliography

[1] H.C. Meng, K.C. Ludema, Wear models and predictive equations: their form and content, Wear. 181–183 (1995) 443–457. doi:10.1016/0043-1648(95)90158-2.

[2] S. Guadalupe Maldonado, S. Mischler, M. Cantoni, W.-J. Chitty, C. Falcand, D. Hertz, Mechanical and chemical mechanisms in the tribocorrosion of a Stellite type alloy, Wear. (2013). doi:10.1016/j.wear.2013.04.007.

[3] J.F. Archard, W. Hirst, The Wear of Metals under Unlubricated Conditions, Proc. R. Soc. Lond. Ser. Math. Phys. Sci. 236 (1956) 397–410. doi:10.1098/rspa.1956.0144.

[4] S. Mischler, A. Spiegel, D. Landolt, The role of passive oxide films on the degradation of steel in tribocorrosion systems, Wear. 225–229, Part 2 (1999) 1078–1087. doi:10.1016/S0043-1648(99)00056-3.

[5] I. Garcı´a, D. Drees, J.P. Celis, Corrosion-wear of passivating materials in sliding contacts based on a concept of active wear track area, Wear. 249 (2001) 452–460. doi:10.1016/S0043-1648(01)00577-4.

[6] A. Bidiville, M. Favero, P. Stadelmann, S. Mischler, Effect of surface chemistry on the mechanical response of metals in sliding tribocorrosion systems, Wear. 263 (2007) 207–217. doi:10.1016/j.wear.2007.01.066.

[7] V. Dalbert, N. Mary, B. Normand, C. Verdu, T. Douillard, S. Saedlou, The effects of microstructures and repassivation kinetics on the tribocorrosion resistance of ferrite and ferrite-martensite stainless steels, Wear. (2018). doi:10.1016/j.wear.2018.10.023.

[8] P. Jemmely, S. Mischler, D. Landolt, Tribocorrosion behaviour of Fe–17Cr stainless steel in acid and alkaline solutions, Tribol. Int. 32 (1999) 295–303. doi:10.1016/S0301-679X(99)00051-1.

[9] C.-O.A. Olsson, D. Landolt, Passive films on stainless steels—chemistry, structure and growth, Electrochimica Acta. 48 (2003) 1093–1104. doi:10.1016/S0013-4686(02)00841-1.

[10] B. Elsner, A.M. Rossi, Effect of pH on Electrochemical Behaviour and Passive Film Composition of Stainless Steels, Mater. Sci. Forum. 192–194 (1995) 225–236. doi:10.4028/www.scientific.net/MSF.192-194.225.

[11] S. Tanaka, N. Hara, K. Sugimoto, Corrosion characteristics of Fe2O3·Cr2O3 artificial passivation films under potentiostatic control, Mater. Sci. Eng. A. 198 (1995) 63–69. doi:10.1016/0921-5093(95)80059-4.

[12] K. Sugimoto, S. Matsuda, Passive and transpassive films on Fe·Cr alloys in acid and neutral solutions, Mater. Sci. Eng. 42 (1980) 181–189. doi:10.1016/0025-5416(80)90027-0.

[13] N. Sato, An overview on the passivity of metals, Corros. Sci. 31 (1990) 1–19. doi:10.1016/0010-938X(90)90086-K.

[14] C.T. Liu, J.K. Wu, Influence of pH on the passivation behavior of 254SMO stainless steel in 3.5% NaCl solution, Corros. Sci. 49 (2007) 2198–2209. doi:10.1016/j.corsci.2006.10.032.

[15] P. Ponthiaux, F. Wenger, D. Drees, J.P. Celis, Electrochemical techniques for studying tribocorrosion processes, Wear. 256 (2004) 459–468. doi:10.1016/S0043-1648(03)00556-8.

[16] N. Papageorgiou, S. Mischler, Electrochemical Simulation of the Current and Potential Response in Sliding Tribocorrosion, Tribol. Lett. 48 (2012) 271–283. doi:10.1007/s11249-012-0022-9.

[17] J.L. Gilbert, S.A. Mali, Y. Liu, Area-dependent impedance-based voltage shifts during tribocorrosion of Ti-6Al-4V biomaterials: theory and experiment, Surf. Topogr. Metrol. Prop. 4 (2016) 034002. doi:10.1088/2051-672X/4/3/034002.

[18] K. Hladky, J.L. Dawson, The measurement of corrosion using electrochemical 1f noise, Corros. Sci. 22 (1982) 231–237. doi:10.1016/0010-938X(82)90107-X.

[19] A. Berradja, D. Déforge, R.P. Nogueira, P. Ponthiaux, F. Wenger, J.-P. Celis, An electrochemical noise study of tribocorrosion processes of AISI 304 L in Cl − and media, 39 (2006) 3184–3192. doi:10.1088/0022-3727/39/15/S08.

[20] P. Jemmely, S. Mischler, D. Landolt, Electrochemical modeling of passivation phenomena in tribocorrosion, Wear. 237 (2000) 63–76. doi:10.1016/S0043-1648(99)00314-2.

[21] C.-O.A. Olsson, M. Stemp, Modelling the transient current from two rubbing electrode configurations: insulating pin on metal substrate and metal pin on insulating substrate, Electrochimica Acta. 49 (2004) 2145–2154. doi:10.1016/j.electacta.2003.12.041.

[22] G.T. Burstein, P.I. Marshall, Growth of passivating films on scratched 304L stainless steel in alkaline solution, Corros. Sci. 23 (1983) 125–137. doi:10.1016/0010-938X(83)90111-7.

[23] T.A. Adler, R.P. Walters, Repassivation of 304 Stainless Steel Investigated with a Single Scratch Test, Corrosion. 49 (1993) 399–408. doi:10.5006/1.3316067.

[24] D. Landolt, S. Mischler, Tribocorrosion of Passive Metals and Coatings, Elsevier, 2011.

[25] N. Espallargas, R. Johnsen, C. Torres, A.I. Muñoz, A new experimental technique for quantifying the galvanic coupling effects on stainless steel during tribocorrosion under equilibrium conditions, Wear. 307 (2013) 190–197. doi:10.1016/j.wear.2013.08.026.

[26] D. Déforge, F. Huet, R.P. Nogueira, P. Ponthiaux, F. Wenger, Electrochemical Noise Analysis of Tribocorrosion Processes under Steady-State Friction Regime, 62 (2006) 514–521. doi:10.5006/1.3279910.

[27] P.-Q. Wu, J.-P. Celis, Electrochemical noise measurements on stainless steel during corrosion–wear in sliding contacts, Wear. 256 (2004) 480–490. doi:10.1016/S0043-1648(03)00558-1.

[28] V. Dalbert, N. Mary, B. Normand, C. Verdu, T. Douillard, S. Saedlou, The effects of microstructures and repassivation kinetics on the tribocorrosion resistance of ferrite and ferrite-martensite stainless steels, Wear. 420–421 (2019) 245–256. doi:10.1016/j.wear.2018.10.023.

[29] M. Moine, N. Mary, B. Normand, L. Peguet, A. Gaugain, H.N. Evin, Tribo electrochemical behavior of ferrite and ferrite–martensite stainless steels in chloride and sulfate media, Wear. 292–293 (2012) 41–48. doi:10.1016/j.wear.2012.06.001.

[30] A. de Frutos, M.A. Arenas, G.G. Fuentes, R.J. Rodríguez, R. Martínez, J.C. Avelar-Batista, J.J. de Damborenea, Tribocorrosion behaviour of duplex surface treated AISI 304 stainless steel, Surf. Coat. Technol. 204 (2010) 1623–1630. doi:10.1016/j.surfcoat.2009.10.039.

[31] A.C. Vieira, L.A. Rocha, N. Papageorgiou, S. Mischler, Mechanical and electrochemical deterioration mechanisms in the tribocorrosion of Al alloys in NaCl and in NaNO3 solutions, Corros. Sci. 54 (2012) 26–35. doi:10.1016/j.corsci.2011.08.041.

[32] D. Landolt, S. Mischler, M. Stemp, Electrochemical methods in tribocorrosion: a critical appraisal, Electrochimica Acta. 46 (2001) 3913–3929. doi:10.1016/S0013-4686(01)00679-X.

[33] J. Qu, J.J. Truhan, An efficient method for accurately determining wear volumes of sliders with non-flat wear scars and compound curvatures, Wear. 261 (2006) 848–855. doi:10.1016/j.wear.2006.01.009.

[34] O. Lavigne, C. Alemany-Dumont, B. Normand, S. Berthon-Fabry, R. Metkemeijer, Thin chromium nitride PVD coatings on stainless steel for conductive component as bipolar plates of PEM fuel cells: Ex-situ and in-situ performances evaluation, Int. J. Hydrog. Energy. 37 (2012)

10789–10797. doi:10.1016/j.ijhydene.2012.04.035.
[35] A. Stachowiak, W. Zwierzycki, Tribocorrosion modeling of stainless steel in a sliding pair of pin-on-plate type, Tribol. Int. 44 (2011) 1216–1224. doi:10.1016/j.triboint.2011.05.020.
[36] A. Dalmau, A.R. Buch, A. Rovira, J. Navarro-Laboulais, A.I. Muñoz, Wear model for describing the time dependence of the material degradation mechanisms of the AISI 316L in a NaCl solution, Wear. 394–395 (2018) 166–175. doi:10.1016/j.wear.2017.10.015.
[37] B.A. Okorie, Kinetics of Formation of Passive Oxide Films on Corrosion-Resistant Fe-Cr Thin Films, J. Electrochem. Soc. 130 (1983) 290. doi:10.1149/1.2119696.
[38] Repassivation rates of surgical implant alloys by rotating‐disk scratching measurements - Frangini - 2001 - Materials and Corrosion - Wiley Online Library, (n.d.). https://onlinelibrary.wiley.com/doi/abs/10.1002/1521-4176(200105)52:5%3C372::AID-MACO372%3E3.0.CO;2-O (accessed July 10, 2019).
[39] C.-O.A. Olsson, D. Hamm, D. Landolt, Evaluation of Passive Film Growth Models with the Electrochemical Quartz Crystal Microbalance on PVD Deposited Cr, J. Electrochem. Soc. 147 (2000) 4093. doi:10.1149/1.1394025.
[40] G.T. Burstein, P.I. Marshall, The coupled kinetics of film growth and dissolution of stainless steel repassivating in acid solutions, Corros. Sci. 24 (1984) 449–462. doi:10.1016/0010-938X(84)90070-2.
[41] R.S. Lillard, G. Vasquez, D.F. Bahr, The Kinetics of Anodic Dissolution and Repassivation on Stainless Steel 304L in Solutions Containing Nitrate, J. Electrochem. Soc. 158 (2011) C194–C201. doi:10.1149/1.3574367.
[42] T.R. Beck, Electrochemistry of freshly-generated titanium surfaces—II. Rapid fracture experiments, Electrochimica Acta. 18 (1973) 815–827. doi:10.1016/0013-4686(73)85033-9.
[43] J. Camra, E. Bielańska, A. Bernasik, K. Kowalski, M. Zimowska, A. Białas, M. Najbar, Role of Al segregation and high affinity to oxygen in formation of adhesive alumina layers on FeCr alloy support, Catal. Today. 105 (2005) 629–633. doi:10.1016/j.cattod.2005.06.015.
[44] L. Wang, T. Maxisch, G. Ceder, Oxidation energies of transition metal oxides within the $\mathrm{GGA}+\mathrm{U}$ framework, Phys. Rev. B. 73 (2006) 195107. doi:10.1103/PhysRevB.73.195107.
[45] P. Radhakrishnamurty, P. Adaikkalam, pH-potential diagrams at elevated temperatures for the chromium/water system, Corros. Sci. 22 (1982) 753–773. doi:10.1016/0010-938X(82)90012-9.
[46] A. Stefánsson, Iron(III) Hydrolysis and Solubility at 25 °C, Environ. Sci. Technol. 41 (2007) 6117–6123. doi:10.1021/es070174h.
[47] D.D. Macdonald, The history of the Point Defect Model for the passive state: A brief review of film growth aspects, Electrochimica Acta. 56 (2011) 1761–1772. doi:10.1016/j.electacta.2010.11.005.
[48] X.Y. Wang, D.Y. Li, Application of an electrochemical scratch technique to evaluate contributions of mechanical and electrochemical attacks to corrosive wear of materials, 259 (2005) 1490–1496. doi:10.1016/j.wear.2005.02.041.
[49] Z. Doni, A.C. Alves, F. Toptan, J.R. Gomes, A. Ramalho, M. Buciumeanu, L. Palaghian, F.S. Silva, Dry sliding and tribocorrosion behaviour of hot pressed CoCrMo biomedical alloy as compared with the cast CoCrMo and Ti6Al4V alloys, Mater. Des. 1980-2015. 52 (2013) 47–57. doi:10.1016/j.matdes.2013.05.032.
[50] S. Cao, S. Guadalupe Maldonado, S. Mischler, Tribocorrosion of passive metals in the mixed lubrication regime: theoretical model and application to metal-on-metal artificial hip joints,

Wear. 324 (2015) 55–63. doi:10.1016/j.wear.2014.12.003.

[51] S. Cao, S. Mischler, Assessment of a recent tribocorrosion model for wear of metal-on-metal hip joints: Comparison between model predictions and simulator results, Wear. 362–363 (2016) 170–178. doi:10.1016/j.wear.2016.05.025.

[52] I. Olefjord, L. Wegrelius, Surface analysis of passive state, Corros. Sci. 31 (1990) 89–98. doi:10.1016/0010-938X(90)90095-M.

[53] V. Maurice, W.P. Yang, P. Marcus, XPS and STM Study of Passive Films Formed on Fe‐22Cr(110) Single‐Crystal Surfaces, J. Electrochem. Soc. 143 (1996) 1182–1200. doi:10.1149/1.1836616.

[54] L. Freire, M.J. Carmezim, M.G.S. Ferreira, M.F. Montemor, The passive behaviour of AISI 316 in alkaline media and the effect of pH: A combined electrochemical and analytical study, Electrochimica Acta. 55 (2010) 6174–6181. doi:10.1016/j.electacta.2009.10.026.

[55] S. Haupt, H.-H. Strehblow, A combined surface analytical and electrochemical study of the formation of passive layers on FeCr alloys in 0.5 M H2SO4, Corros. Sci. 37 (1995) 43–54. doi:10.1016/0010-938X(94)00104-E.

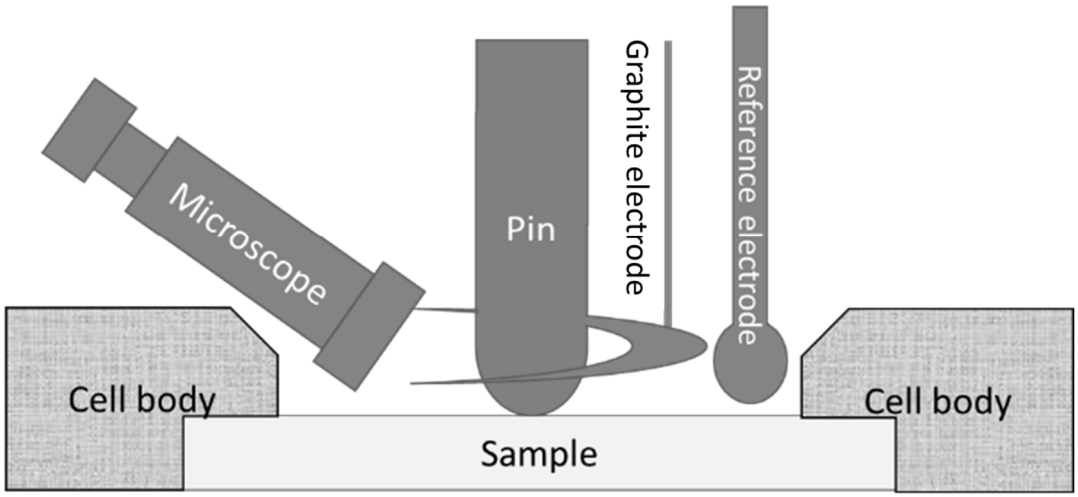

Figure 1. Schematic representation of the tribocorrosion cell with the implementation of the optical microscope, the half-moon shape graphite electrode, the reference electrode and the corundum pin. The cell volume is equal to 40 ml.

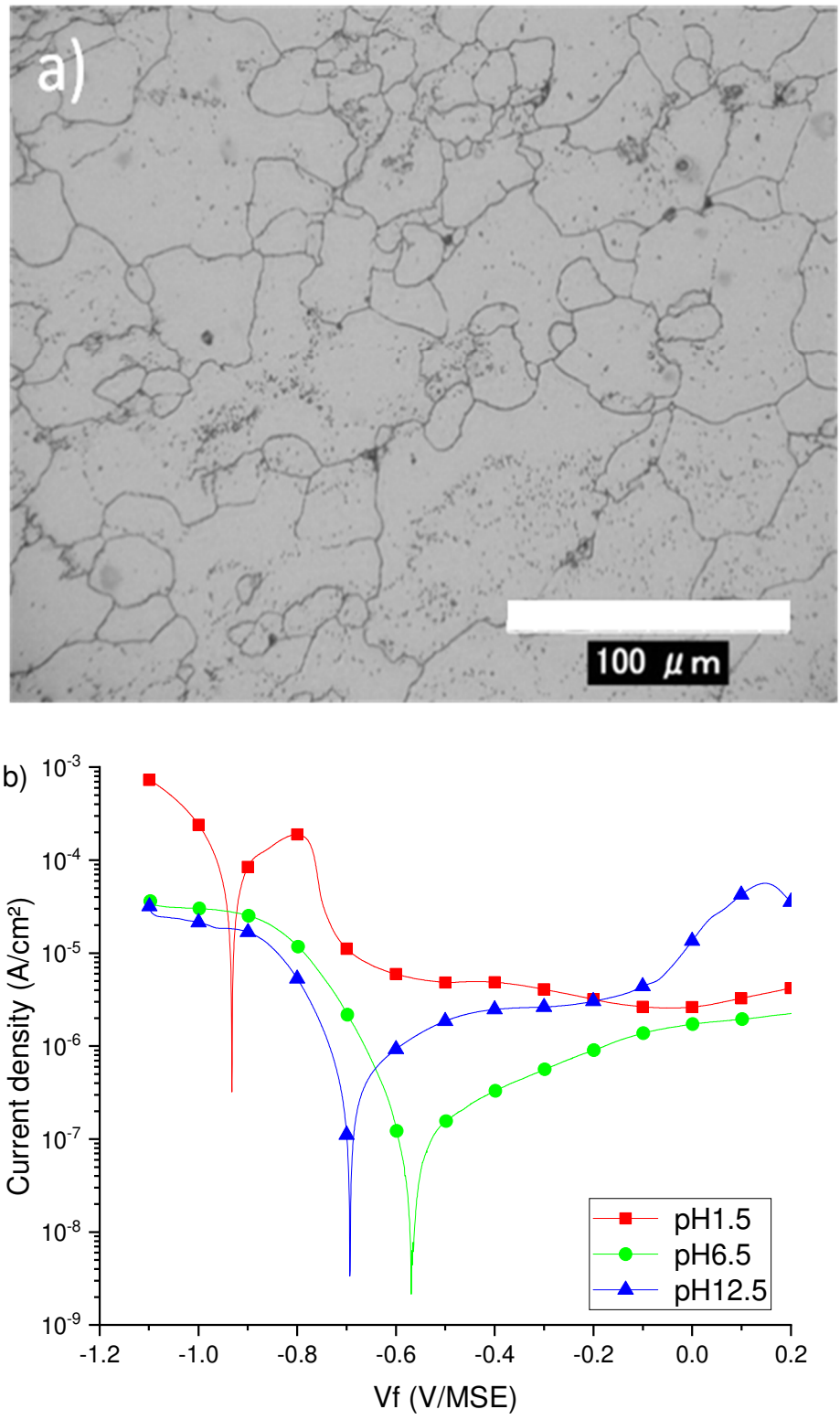

Figure 2. a) Surface of AISI430 microstructure after electrochemical etching and b) polarization curves recorded for different pH after a storage in dry atmosphere for 24 hours and a cathodic pre-polarization step.

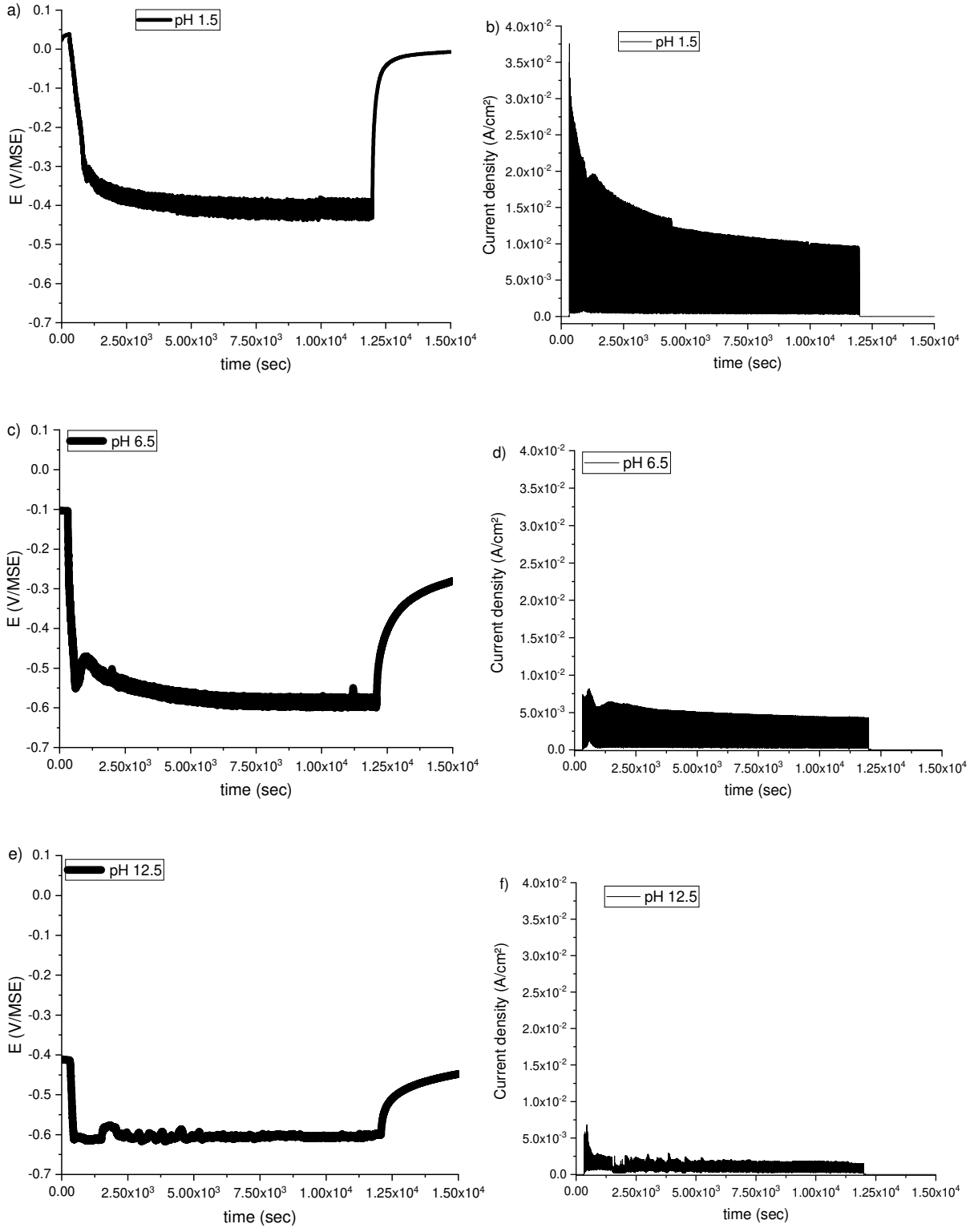

Figure 3. Potentials (left column) and current densities (right column) variations during tribocorrosion experiments in solution (a, b) pH 1.5, (c, d) pH 6.5 and (e, f) pH 12.5.

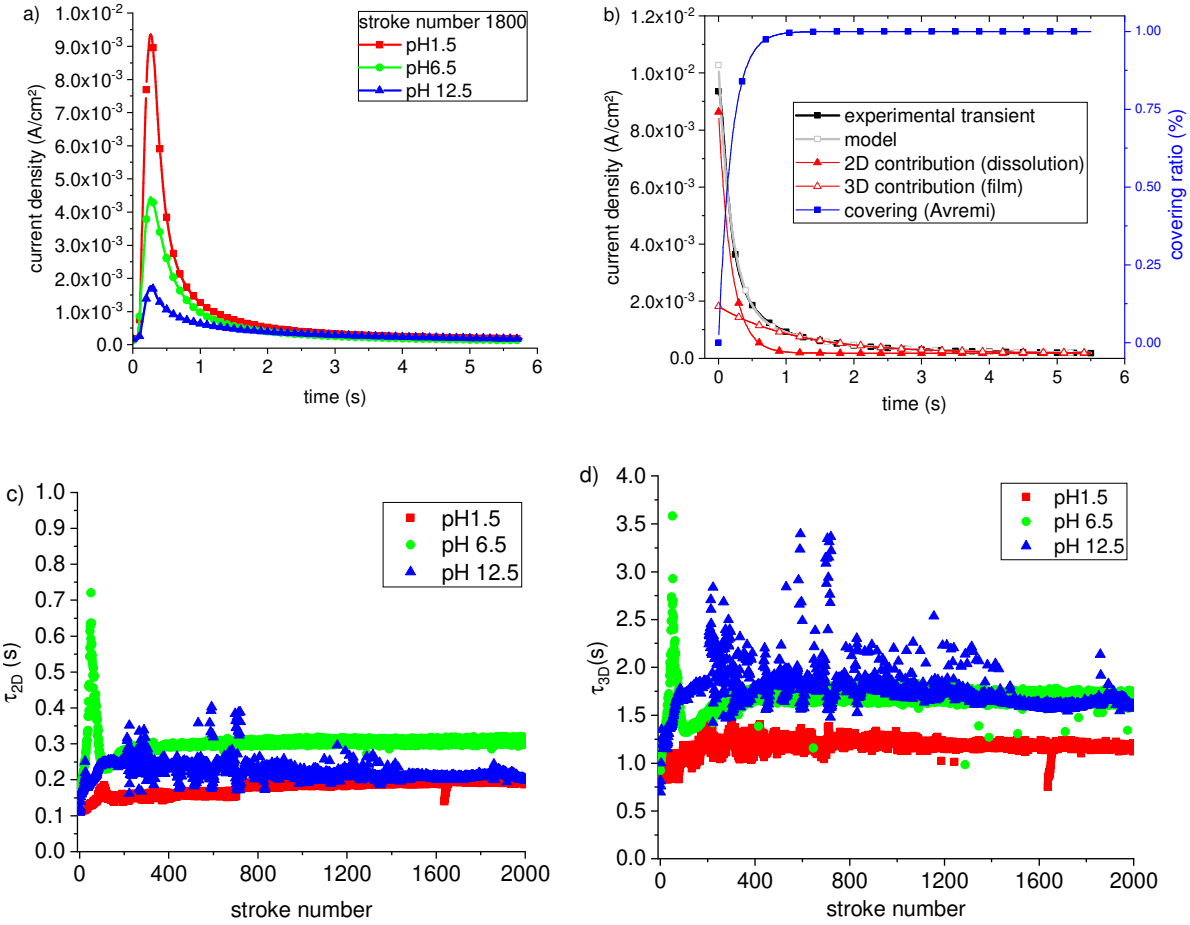

Figure 4. a) single current transient extracted from Figure 3 (stroke number 1800) and b) modeling of the repassivation transient at pH1.5 after 1800 sliding (Equation 2) and covering rate of the fresh surface by passive film nuclei (Equation 3). Variations of c) τ_{2D} and c) τ_{3D} with the stroke number. All fits were obtained with a χ^2 higher than 0.98.

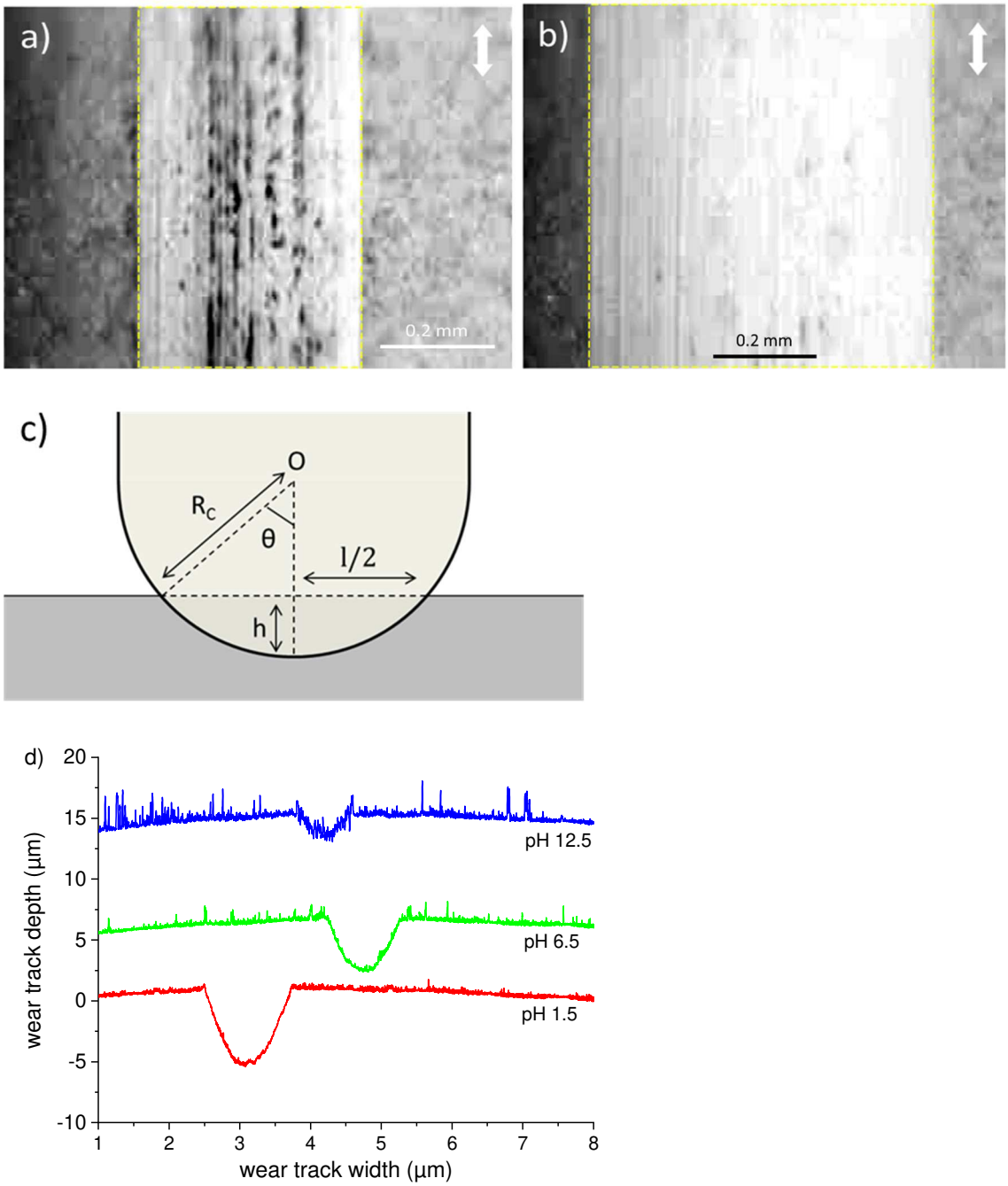

Figure 5. Wear track images after b) 180 and c) 1480 sliding in acidic solution. d) Description of the pin penetration model and d) wear track profiles after tribocorrosion tests

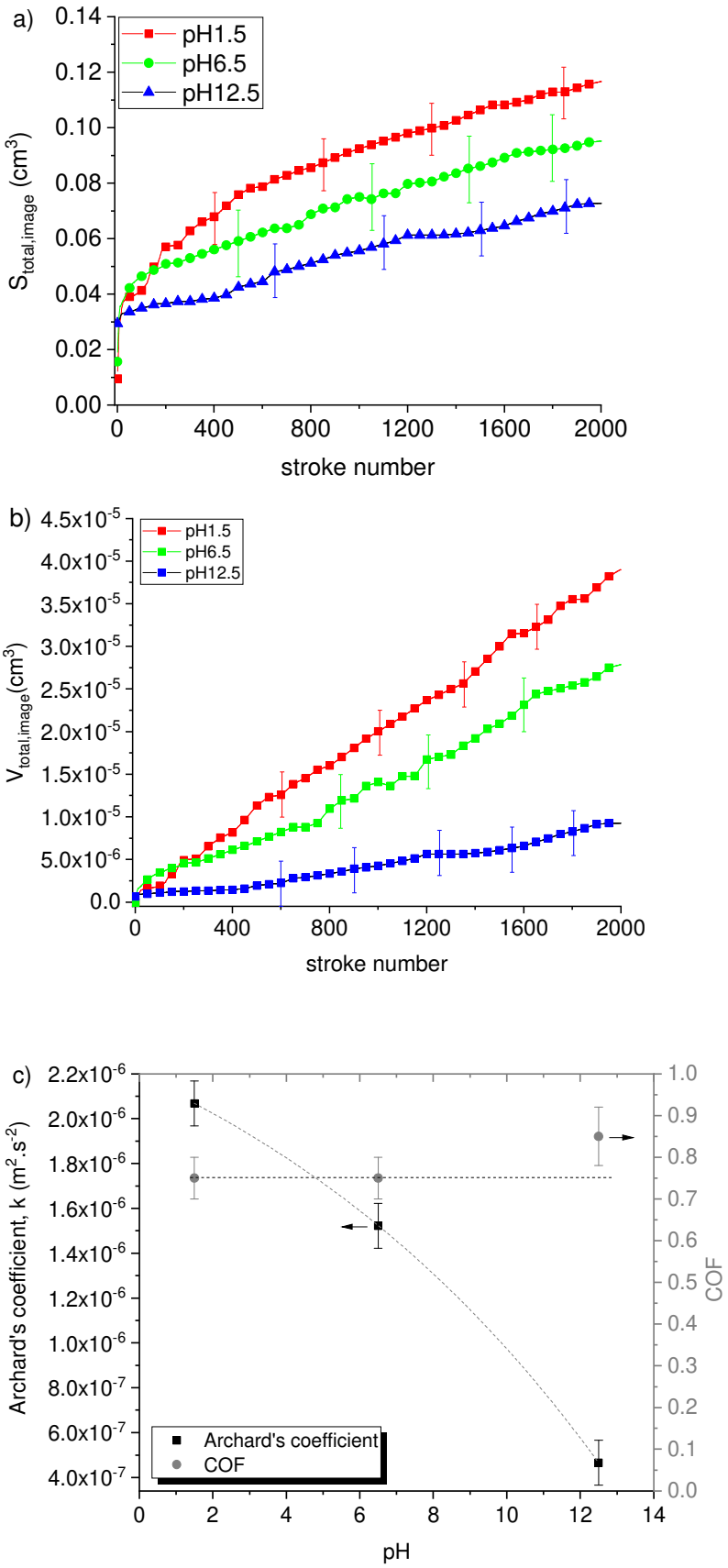

Figure 6. Variations of a) the wear surface and b) the wear volume determined from the optical observations of the wear tracks as a function of the solution pH. c) Average coefficient of friction (COF) and Archard's coefficient as a function of pH

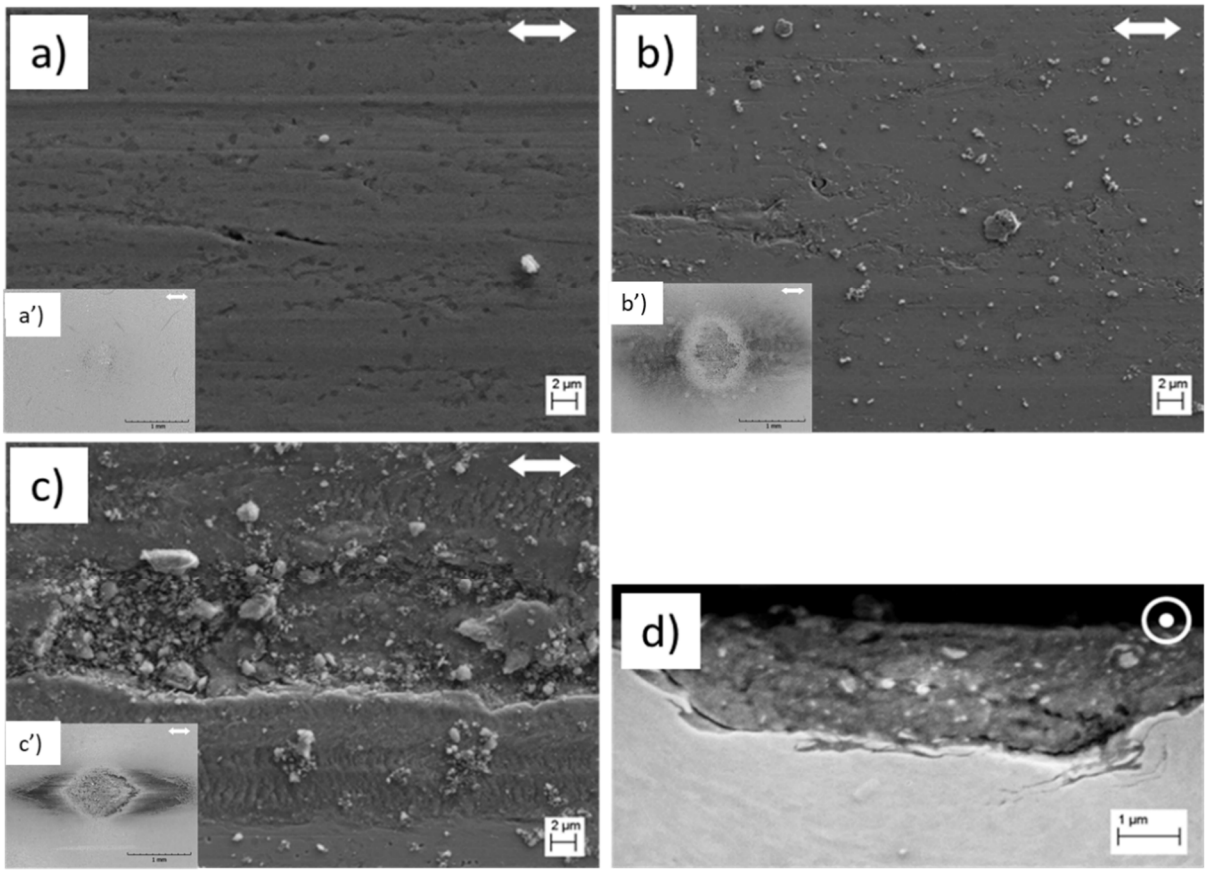

Figure 7. SEM observations of the worn surfaces in a) pH 1.5, b) pH 6.5 and c) pH 12.5. d) cross section observation of the wear track at pH 12.5. Pin surfaces are in the windows images.

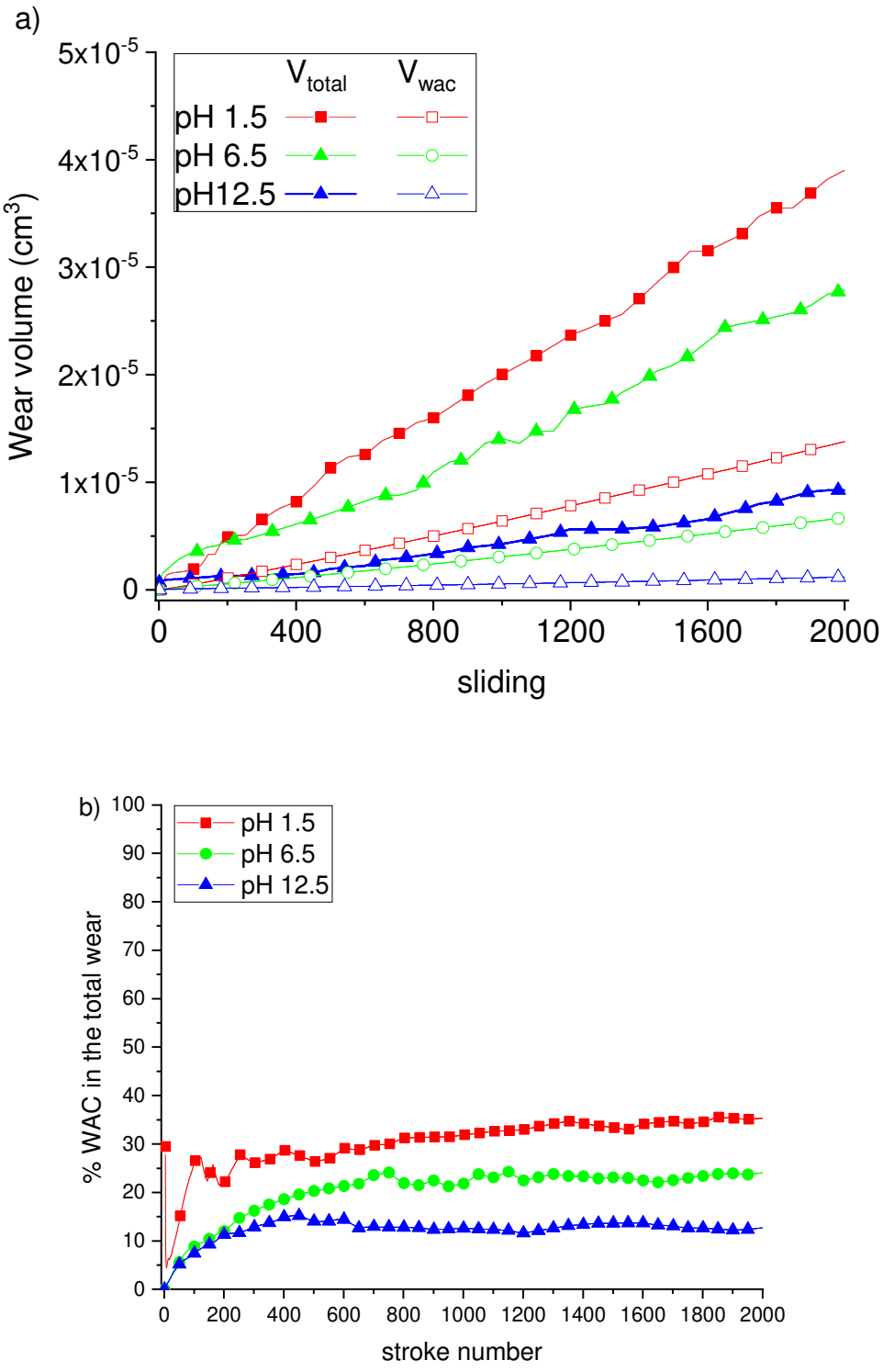

Figure 8. a) Comparison between the total wear volume and the Wear-accelerated corrosion volume (WAC), b) contribution of WAC in the total wear.

Table 1. Repassivation time constants (τ_{2D} and τ_{3D}), wear surfaces and volumes from the analysis of optical images recorded along the sliding ($S_{total,image}$, $V_{total,image}$) and 2D profiles recorded after the experiments ($S_{total,\ 2Dprofile}$, $V_{total,\ profile}$).

pH	Time constant (s) ± *0.01*		Wear surfaces (cm^2) ± 0.01		Wear Volumes (x 10^{-5} cm^3) ±0.3 x10^{-5}	
	τ_{2D}	τ_{3D}	$S_{total,image}$	$S_{total,2Dprofile}$	$V_{total,2Dprofile}$	$V_{total,image}$
1.5	0.19	1.18	0.11	0.12	3.8	4.0
6.5	0.30	1.69	0.09	0.09	2.8	2.7
12.5	0.21	1.67	0.07	0.08	0.9	0.9